PLASTIC DESIGN OF HOT-FINISHED HIGH STRENGTH STEEL CONTINUOUS BEAMS

Michaela Gkantou, Marios Theofanous and Charalampos Baniotopoulos

School of Engineering, Civil Engineering Department, The University of Birmingham, Edgbaston, B15 2TT, Birmingham, United Kingdom

Keywords: High strength steel, hot-finished, hollow sections, continuous beams, Eurocode, plastic design

Abstract. *High strength steels (HSS) are increasingly used in structural engineering applications owing to their high strength to weight ratio. Due to the inferior ductility and strain-hardening characteristics of HSS and the lack of relevant structural performance data, plastic design is currently not permitted for HSS indeterminate structures. To this end, the present paper aims to generate structural performance data and to assess the applicability of plastic design to hot-finished HSS continuous beams. Upon a summary of previously drawn conclusions regarding the applicability of European design provisions to S460 and S690 hot-finished square and rectangular hollow sections, a gap on the response and design of indeterminate structures is identified. Validated numerical models of two-span HSS continuous beams are subsequently used for the generation of a wide range of structural performance data by developing a broad parametric studies numerical program. The effect of key parameters such as the cross-section slenderness, the cross-section aspect ratio and the steel grade on the structural response of continuous beams is assessed. The obtained results are discussed and the possibility of plastic design for high strength steel indeterminate structures is evaluated, whilst reliability of the elastic and plastic design methods is also verified according to Annex D of EN 1990.*

1 INTRODUCTION

Structural steels with yield strengths over 460 N/mm^2, known as high strength steels (HSS) in building sector, can be achieved by appropriate heat treatments that improve its material and mechanical properties. Normalising (N), quenching and tempering (QT) and thermomechanical controlled rolling process (TMCP) are the most common heat treatments applied for the development of high strength steels. N produces rolled sections of moderate strength up to 460 N/mm^2, QT results in very high strength steel plates up to 1100 N/mm^2, whilst TMCP sections can have a yield strength up to 690 N/mm^2. QT steel plates are commonly known as ultra or very high strength steel plates, while TMCP generally produces rolled steel with high toughness properties and better weldability than ordinary steel.

HSS applications can potentially lead to lighter structures, considerable sustainability gains and more economic design. In order to maximise these benefits and increase the usage of HSS in the construction industry, appropriate design guidance in line with the observed structural response needs to be available. The European provisions for HSS structural design are set out in EN 1993-1-12 [1] and in most cases adopt the design provisions codified in EN 1993-1-1 [2] for conventional steel structures. Despite the significant

differences in material ductility and strain-hardening characteristics between high strength and mild steel, HSS design provisions are largely based on test data for mild steel. Hence, the suitability of current design provisions to HSS requires assessment.

Towards this direction, numerous experimental and numerical programmes have been conducted in order to determine the structural response of HSS cross-sections, individual members and structures, and estimate the suitability of design specifications to HSS. In particular, research studies on HSS long columns [3-6], stub columns [7,8] and beams [9-11] have been carried out. It is noteworthy that studies on the behaviour of HSS members with a nominal yield strength exceeding 1000 N/mm^2 have also been reported [12, 13]. Most of the aforementioned studies have focused on the performance of cold-formed and welded HSS sections, leaving the performance of hot-finished cross-sections relatively unexplored. The fact that focus has been placed on cold-formed and welded HSS sections is mainly related to the residual stresses that could be significant in those cases, affecting the ultimate performance. However, as demonstrated in past studies [14-16], the ultimate structural performance is related to the ratio of the residual stresses to the yield strength and not the magnitude of the residual stresses themselves, which appear similar for mild and high strength steels. Therefore, the influence of the residual stresses is expected to decrease for increasing steel grades, while the effect of the reduced strain-hardening and ductility of higher steel grades remains. The latter means that the effect of the material response of HSS needs to be considered also for hot-finished sections, where the final processing is performed using high temperature thermal treatment, resulting in lower residual stresses. Hence, the investigation of the structural performance of HSS hot-finished hollow sections is warranted.

To this end, an extensive experimental programme [17-22] has been recently carried out in order to evaluate the ultimate performance of structures employing square and rectangular hot-finished hollow sections in S460 and S690 steel grades. The present paper initially summarises the conclusions and design recommendations regarding the applicability of European design provisions to HSS hot-finished hollow sections resulting from this recent research programme. A knowledge gap regarding the response and design of HSS indeterminate structures is thus identified. Aiming to address the lack of design guidance and structural performance data for HSS indeterminate structures, a comprehensive finite element (FE) parametric study on HSS continuous beams is reported herein. It is noteworthy that even though the structural performance of continuous beams made from mild steel [23,24], aluminium alloys [25-27] and stainless steels [28-30] has been studied, research on high strength steel continuous beams has not been reported yet. Thus upon numerical analyses execution, the possibility to extend conventional plastic design rules to high strength steel indeterminate structures is discussed.

2 RESEARCH PROGRAMME ON HOT-FINISHED HOLLOW SECTION MEMBERS

2.1 Overview of the research programme [17-22]

A series of experimental and numerical studies have been performed to investigate the structural response of HSS structures. Two steel grades, namely S460 and S690 on square and rectangular hollow sections, were examined. The sections were hot-rolled, seamlessly fabricated from continuously cast round ingots and hollowed out in a piercing mill to their final section shape. The high strength of the sections in Grade S460 was achieved with the normalising process, whilst for the S690 sections the quenching and tempering processes were used. The research programme is summarised in Table 1, where the structural components studied, the number of experiments and the number of FE analyses performed along with the parameters investigated are listed.

It is worth noting that the structural components studied in [17-21] were expected to fail by local buckling. In order to treat local buckling, Eurocode -as most modern structural design codes- makes use of the cross-section classification procedure. Based on the comparison of their width-to-thickness ratio (i.e. $c/t\varepsilon$, where c is the compressed flat width, t is the plate thickness and $\varepsilon=(235/f_y)^{0.5}$ with f_y being the material yield strength) against codified slenderness limits, the constituent plated elements comprising the cross-sections are placed in one of four behavioural groups termed classes, and the cross-section is classified as its least favourably classified element [2]. Therefore, one critical parameter considered for the individual structural components is the cross-section slenderness. Details on related research are provided in [17-22].

Table 1. Summary of research programme [17-22].

Structure	No of Experiments	No of FE Parametric Studies	Parameters
Stub columns under concentric compression [17, 18]	11	180	• Fifteen cross-section slendernesses • Six cross-section aspect ratios • Two steel grades
Beams loaded in the three-point and four-point bending configuration [19]	22	216	• Twelve cross-section slendernesses • Three cross-section aspect ratios • 3-point with L/h=10, 3-point with L/h=20, 4-point with L/h=20 • Two steel grades
Stub columns under combined compression and uniaxial bending [20]	12	720	• Eight cross-section slendernesses • Three cross-section aspect ratios • Nine loading eccentricities • Two bending axes for the rectangular hollow sections • Two steel grades
Stub columns under combined compression and biaxial bending [21]	-	1376	• Eight cross-section slenderness • Two cross-section aspect ratios • Forty-three loading eccentricities - bending about both axes • Two steel grades
Long columns under concentric compression [22]	30	144	• Three cross-section slendernesses • Two cross-section aspect ratios • Eight column slendernesses • Two buckling axes • Two steel grades

2.2 Eurocode assessment on the basis of the results

The obtained results of the research programme [17-22] were used to assess the applicability of Eurocode design specifications [1, 2] to HSS. A summary of the Eurocode assessment is presented in Table 2 and explained briefly herafter.

In [18] it was shown that the application of the Eurocode effective width equations [31] led to rather conservative strength estimations for rectangular hollow sections with high aspect ratios. To overcome this issue, the effective cross-section method was presented. The new approach suggests a reduction factor applied to the whole cross-sectional area (and not to each constituent plate element) and yields safe yet economic design estimations for hollow sections with different aspect ratios.

In order to assess the Eurocode provisions for the cross section capacity under interactive bending and compression, the test or FE to the predicted capacity ratio ($R_{test/FE}/R_{pred}$) was used in [20,21]. Points outside

the boundary of the design curve (or surface) correspond to capacities higher than the predicted one (i.e. utilisation ratio higher than unity) and lead to safe predictions. The comparison displayed generally sufficiently accurate predictions.

The results of [22] were used to assess the applicability of flexural buckling formulae to HSS. A reliability analysis revealed that current European specifications are suitable for hot-finished S460 and S690 SHS and RHS columns as long as a safety factor γ_{M1} equal to 1.1 applies.

Table 2. Summary of Eurocode assessment.

Provision assessed	Description	Author [Ref]	Research Outcome
Eqs. (4.1)-(4.3) of [31]	Effective width equations for Class 4 cross sections	[18]	• Current equations safe but conservative estimations for large *H/B* • New design equations proposed
Eqs. (6.31)-(6.32) and (6.39)-(6.44) of [2]	Cross section capacity under interactive bending and compression	[20, 21]	• Overall safe predictions
Eq. (6.46)-(6.51) and Tables 6.1-6.2 of [2]	Flexural buckling under concentric compression	[22]	• Overall safe predictions for γ_{M1}=1.1
Table 5.2 of [2]	Eurocode slenderness limits for internal elements	[17-19]	• For internal elements in compression: proposed Class 2 limit: 34; proposed Class 3 limit: 38 • For internal elements in bending: current limits acceptable
Eq. (6.14) of [2]	Bending moment capacity for Class 3 cross sections	[20, 21]	• Linear transition between M_{pl} to M_{el}
Table 5.2 of [2] along with [19]	Rotation capacity requirements	[19]	• Proposed Class 1 limit: 28 • Further research needed

In order to assess the applicability of the Eurocode Class 2 and Class 3 limits for internal elements in compression to HSS, the relationship between the experimental bending moment to plastic moment ratio and the slenderness of the compressive flange was examined in [19]. The applicability of the current Eurocode Class 2 of 38 and Class 3 limit of 42 to HSS appeared problematic. Revised Class 2 and Class 3 limits of 34 and 38 respectively were proposed for internal elements in compression. Current Eurocode Class 2 of 83 and Class 3 limit of 124 for internal elements in bending appeared adequate for the studied HSS sections.

According to Eurocode, the design resistance for bending of a Class 3 cross-section is equal to its elastic moment resistance about the relevant bending axis. However, past research [19-21] has shown that this assumption yields quite conservative strength predictions. More economic yet safe strength estimations for Class 3 sections can be produced assuming a linear strength transition between Class 2 and Class 4 sections in the semi-compact design. This is introduced through a relationship between the bending strength and the $c/t\varepsilon$ slenderness of the cross-section, varying linearly from the plastic moment resistance $M_{pl,Rd}$ for cross-sections with $c/t\varepsilon$ equal to the Class 2 limit to the elastic moment resistance $M_{el,Rd}$ for cross-sections with $c/t\varepsilon$ equal to the Class 3 limit. Adopting the aforementioned concept for Class 3 sections, the average value of the ultimate normalised moment capacity falls from 1.17 to 1.06 for hot-finished HSS beams. Similarly, for stub columns under uniaxial bending and compression, the utilisation ratio falls from 1.15 to 1.09 [20],

while the respective ratio decreases from 1.37 to 1.14 for semi-compact stub columns subjected to biaxial bending and compression [21].

The results on HSS beams [19] have also been used to evaluate the rotation capacity of HSS. The rotation capacity is relevant to Class 1 sections (i.e. sections that are able to form a plastic hinge without a reduction of their capacity below their plastic moment resistance). It can be viewed as the exploitation level of the inelastic range of the material stress-strain curve under monotonic static loading and is thus closely related to the material ductility. This is particularly important in plastic design, where the structural system should carry high loads that induce inelastic deformation and the structure should have sufficient plastic deformation capacity in order to form a collapse mechanism. According to Eurocode, the rotation capacity of a 3-point beam can be estimated by $R=\theta_u/\theta_{pl}$ *-1*, where θ_{pl} is the elastic part of the total rotation at mid-span when M_{pl} is attained on the ascending branch, whilst θ_u is the total rotation at mid-span when the moment-rotation curve falls back below M_{pl}. Even though 1993-1-12 [1] suggests that for HSS structures "the global analysis using non-linear plastic analysis considering partial plastification of members in plastic zones only, applies", thereby practically not allowing traditional plastic design for high strength steels, the results on HSS hollow section beams [19] have been used for the assessment of the Class 1 limit along with a deformation capacity requirement equal to 3 proposed in [32] and a slenderness limit of 33, which are applied for normal strength steel in EN 1993-1-1 [2]. It was found that the current limit of 33, recommended for mild steel, appears questionable not only for HSS sections but also for ordinary carbon steel sections, while the proposed limit of 28 [19] seems more appropriate, leaving only some results below the rotation capacity requirement. Given though that most of the results -mainly of S460 grade- have achieved significant rotation capacity, further research into the possibility of allowing the use of plastic design for high strength steel structures has been recommended [19].

Aiming to investigate the latter issue, the present paper examines numerically the response of S460 and S690 two-span continuous beams. The results are used to assess the possibility of applying plastic design rules to high strength steel indeterminate structures, which is currently not allowed by 1993-1-12 [1].

3 NUMERICAL MODELLING OF HSS CONTINUOUS BEAMS

3.1 Previously validated FE Models

A numerical model of two-span continuous beams under a set of point loads has been developed using the general purpose FE software ABAQUS [33]. The FE model has been successfully validated against experimental results on stainless steel continuous beams [30], whilst the material properties employed in the models have been obtained from physical tests [19] and used in the past in similar numerical studies on stub columns and beams [18-21]. Figure 1(a) shows a typical load-displacement curve from the validation of the numerical models of continuous stainless steel beams, while Figure 1(b) a typical normalised moment-normalised rotation curve from the validation of the numerical models of simply-supported high strength steel beams under 3-point bending. A very good agreement between the experimental and numerical response in terms of initial stiffness, ultimate load, post-ultimate response and failure modes has been observed in studies [18-20,30]. A summary of the obtained ratios of the FE to test ultimate loads ($F_{u,FE}/F_{u,test}$) [18-20,30] is reported in Table 3. Note that previous studies on hot-finished HSS beams coupled with initial geometric imperfection measurements [19], informed the choice of an appropriate geometric imperfection magnitude which was selected as *t/50* for all sections modelled, *t* being the cross-section thickness, and thus the provided ratios in Table 3 correspond to the FE results with the aforementioned geometric imperfection.

In absence of experimental results for high strength steel continuous beams, it can be supported that adopting the same numerical modelling assumptions, the previously validated models can be safely used to investigate numerically the performance of continuous HSS beams.

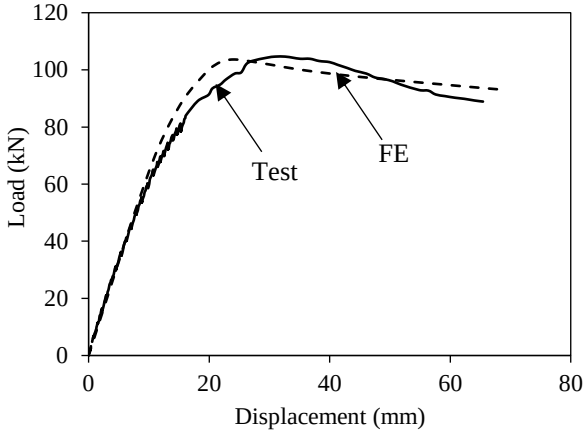

a) Validation of continuous stainless steel beams (adopted from [30])

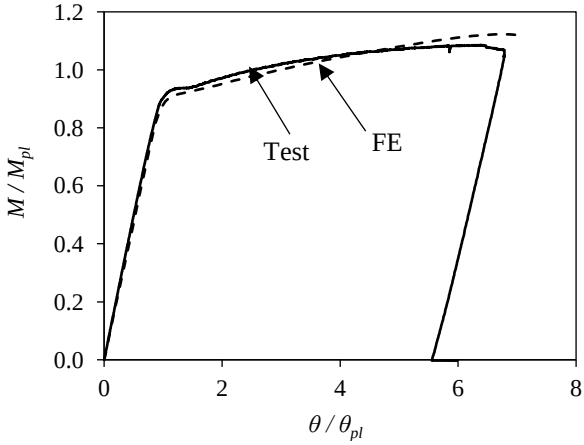

b) Validation of simply-supported high strength steel beams (adopted from [19])

Figure 1. Typical graphs of the validated numerical models.

Table 3. Summary of previously validated numerical models (adopted from [18-20,30])

Type of structure	**Continuous Beams**		Stub Columns		3-point beams		4-point beams		Stub Columns under eccentric compression	
Material	Stainless Steel		**High Strength Steel**							
	Specimen	$F_{u,FE}/F_{u,test}$	Specimen	$F_{u,FE}/F_{u,test}$	Specimen	$F_{u,FE}/F_{u,test}$	Specimen	$F_{u,FE}/F_{u,test}$	Specimen	$F_{u,FE}/F_{u,test}$
	RHS 100×50×2 (Austenitic)	0.92	S460 50×50×5	0.93	S460 SHS 50×50×5	1.01	S460 SHS 50×50×5	1.04	S460 SHS 50×50×5, ecc: 5 mm	0.93
	RHS 100×50×3 (Austenitic)	1.04	S460 50×50×4	0.85	S460 SHS 50×50×4	1.03	S460 SHS 50×50×4	0.95	S460 SHS 50×50×5, ecc: 10 mm	0.91
	RHS 100×50×5 (Austenitic)	0.90	S460 100×100×5	0.96	S460 SHS 100×100×5	0.95	S460 SHS 100×100×5	0.94	S460 SHS 50×50×5, ecc: 20 mm	0.91
	RHS 100×50×3 (Duplex)	0.95	S460 90×90×3.6	1.01	S460 SHS 90×90×3.6	0.97	S460 SHS 90×90×3.6	0.94	S460 SHS 50×50×5, ecc: 30 mm	0.87
			S460 100×50×6.3	0.95	S460 RHS 100×50×6.3	1.00	S460 RHS 100×50×6.3	0.97	S690 SHS 50×50×5, ecc: 5 mm	0.94
			S460 100×50×4.5	0.94	S460 RHS 100×50×4.5	1.06	S460 RHS 100×50×4.5	0.96	S690 SHS 50×50×5, ecc: 10 mm	0.89
			S690 50×50×5	0.90	S690 SHS 50×50×5	0.99	S690 SHS 50×50×5	1.00	S690 SHS 50×50×5, ecc: 15 mm	0.93
			S690 100×100×5.6	1.00	S690 SHS 100×100×5.6	1.00	S690 SHS 100×100×5.6	1.01	S690 SHS 50×50×5, ecc: 20 mm	0.94
			S690 90×90×5.6	0.99	S690 SHS 90×90×5.6	1.02	S690 SHS 90×90×5.6	1.04	S690 SHS 90×90×5.6, ecc: 5 mm	0.93
			S690 100×50×6.3	0.99	S690 RHS 100×50×6.3	1.00	S690 RHS 100×50×6.3	1.01	S690 SHS 90×90×5.6, ecc: 10 mm	0.89
			S690 100×50×5.6	1.00	S690 RHS 100×50×5.6	0.98	S690 RHS 100×50×5.6	0.98	S690 SHS 90×90×5.6, ecc: 25 mm	0.96
									S690 SHS 90×90×5.6, ecc: 30 mm	0.94
Mean		0.98		0.96		1.01		0.99		0.92
COV		0.05		0.05		0.03		0.04		0.03

3.2 Development of the FE Models

Shell elements (i.e. elements that approximate a three-dimensional continuum with a surface model) are commonly used to model structures in which the one dimension is significantly smaller than the other dimensions and the stresses in the thickness direction are negligible. In line with previous studies [27, 34, 35] and with recommendations for FE on metal structures [36], shell elements have been chosen for the modelling of the HSS beams. In particular, the general purpose four-noded shell elements with reduced integration and finite membrane strains S4R, suitable for large-strain analysis, have been used for the discretisation of the structural components. The element formulation of S4R elements allows for transverse shear deformation, by using either thick shell or Kirchhoff theory, depending on the shell thickness, whilst they also allow for finite membrane strains and a change in the shell thickness as a function of the membrane strain [33]. As depicted in Figure 2, curved corner regions were discretised with four elements, while the characteristic element size was set equal to the section's thickness for the flat parts, as previous mesh convergence studies demonstrated its adequacy [18-20]. The effect of the supports was simulated through appropriate boundary conditions and coupling constraints, as shown in Figure 3. The adopted boundary conditions allow rotation in the plane of loading but prevent vertical displacements and have been previously employed in similar studies [30,37]. Due to the symmetry of the configuration with respect to geometry, boundary conditions, loading and failure mode of the continuous beams, only half the cross-section of each specimen was modelled and suitable symmetry boundary conditions were employed along the assumed symmetry axis.

The average material response as extracted from tensile coupon tests [19] and shown in Figure 4(a) has been adopted. The key material properties, including the Young's modulus E, the yield stress f_y, the ultimate stress f_u, the strain at the start of the plateau ε_y, the strain at the start of the strain-hardening region ε_{sh}, and the strain at ultimate stress ε_u, are also reported in Figure 4(b) for both steel grades. As can be observed, the stress-strain curves start with a linear response up to the yield point, followed by a well-defined plateau and a strain-hardening part after it, which is more prominent in the case of S460 than S690. The von Mises yield criterion with isotropic hardening was used. The stress strain curves were converted into the true stress-logarithmic plastic strain format according to Equations (1) and (2) and input into the FE models.

$$\sigma_{true} = \sigma_{eng}\left(1 + \varepsilon_{eng}\right) \tag{1}$$

$$\varepsilon_{ln}^{pl} = \ln\left(1 + \varepsilon_{eng}\right) - \frac{\sigma_{true}}{E} \tag{2}$$

where σ_{eng}, ε_{eng} are the engineering stress and strain respectively, E is the Young's modulus and σ_{true} and ε_{ln}^{pl} are the true stress and logarithmic plastic strain respectively. Initial geometric imperfections were incorporated in the numerical models in form of the lowest elastic buckling mode. Therefore, a linear eigenvalue buckling analysis was initially performed and the buckling mode shapes were extracted. Thereafter, the Riks, which is an arc-length based method, was applied to carry out geometrically and materially nonlinear analysis with imperfections included.

In line with previous studies on hot-finished HSS beams, geometric imperfections with magnitude *t/50*, *t* being the cross-section thickness, have been applied for all sections modelled herein. For the hot-finished HSS sections, residual stress measurements have been performed with the sectioning method [19]. The maximum measured longitudinal membrane residual stresses were found to be $0.055f_y$ in tension and $0.031f_y$ in compression. Owing to their low magnitudes, residual stresses were not explicitly incorporated into the numerical models. The same assumption has been successfully adopted in [18-20].

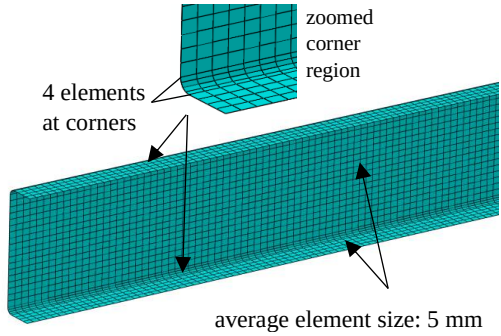

Figure 2. Discretised cross-section – RHS 100×50×5.

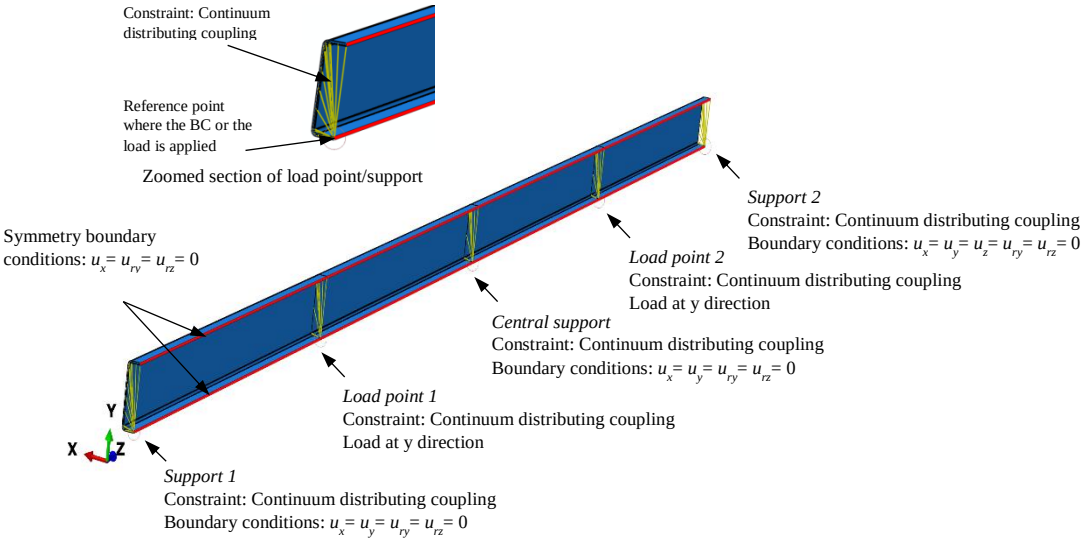

Figure 3. Finite element model along with boundary conditions and constraints applied.

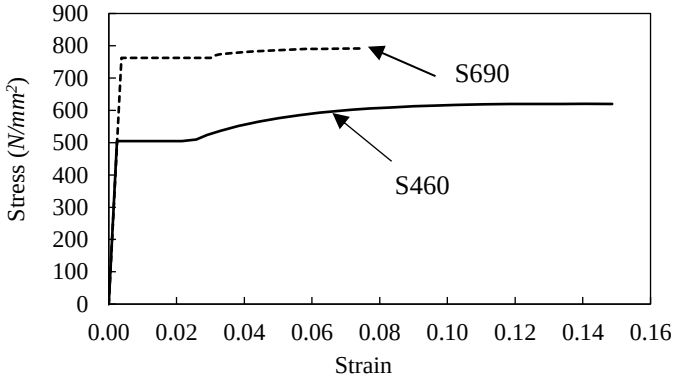

a) Stress-strain curves

Steel grade	E (N/mm^2)	f_y (N/mm^2)	f_u (N/mm^2)	ε_y	ε_{sh}	ε_u
S460	211133	504.93	620.31	0.0024	0.0216	0.148
S690	205602	762.39	791.66	0.0037	0.0295	0.075

b) Key material properties

Figure 4. Material properties of considered HSS grades.

3.2 Parametric studies

In order to investigate the structural performance of continuous beams for various geometric parameters, a series of parametric studies examining the effect of the cross-section slenderness, the cross-section aspect ratio and the steel grade were conducted. Three cross-section aspect ratios *H/B*, where *H* and *B* the section's outer depth and outer width respectively, namely 1.0 *(H=50 mm, B=50 mm)*, 2.0 *(H=100 mm, B=50 mm)* and 2.44 *(H=122 mm, B=50 mm)* were considered. Note that 2.44 is the limit in aspect ratio value that leads to equal slenderness for the compression flange and the web of a hollow section subjected to bending [19]. Moreover, four plate thicknesses, namely 2 *mm*, 3 *mm*, 4 *mm* and 5 *mm*, two material grades, namely S460 and S690, and two load cases were examined. The internal corner radius in all sections was set equal to the cross-sectional thickness. The studied load arrangements along with the considered spans and the corresponding bending moment diagrams at the linear stage are shown in Figure 5. Load Case 1 is the same with that experimentally studied in [30], based on which the numerical models were validated, while Load Case 2 is a typical scenario of two equal spans, loaded equally that has been experimentally examined for two-span continuous beams of other alloys [26-29]. The two load cases lead to different sequence in the formation of the plastic hinges and different moment redistribution, thus providing a broader understanding of the performance of high strength steel continuous beams.

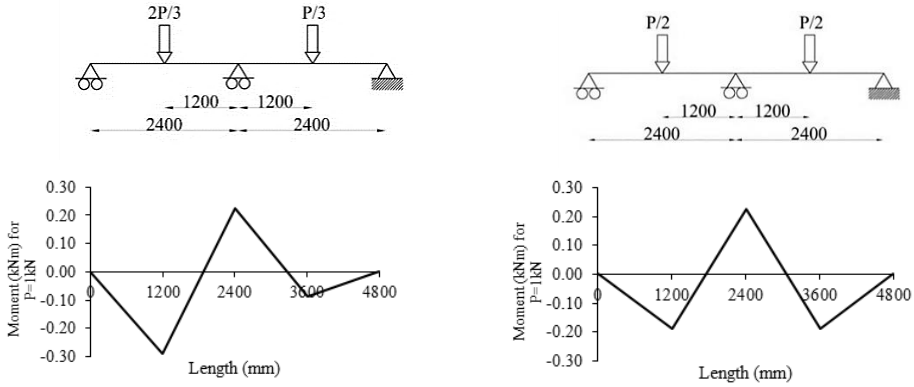

a) Load Case 1 (LC1) – Equal spans; unequal loads b) Load Case 2 (LC2) – Equal spans; equal loads

Figure 5. Load cases studied.

4 DISCUSSION OF RESULTS AND DESIGN RECOMMENDATIONS

4.1 Analysis of the results

For all numerical analyses, the full load-displacement response was tracked. Examining of the tensile strains is important as the inferior ductility of HSS may lead to tensile fracture at the first plastic hinge prior to the formation of the second plastic hinge. This would invalidate the plastic design approach, which is based on availability of sufficient ductility and is the focus of the present study. Hence, the failure load of the models was defined either as the load leading to the formation of two plastic hinges or the load leading to tensile fracture at the most stressed part of the section (i.e. for LC1: bottom of the cross-section at the most loaded point; for LC2: top of the cross-section at the central support). The consideration on the two potential failure mechanisms was in line with past studies on aluminium alloy continuous beams [26,27], in which, as with high strength steels, material ductility should be carefully controlled when evaluating the possibility of plastic design methods.

In absence of experimental data of HSS beams with tensile fracture, but in order to take also this failure mode into account, the tensile fracture is conservatively considered as the dominant failure mode when the maximum allowable strain is achieved at the most stressed part of the structure, before the completion of the plastic hinge formation. Based on the material response shown in Figure 4, the maximum allowable strain values were set equal to 14.8% and 7.5% for S460 and S690 respectively for the beams studied herein. The process applied to define the failure load and mode numerically is as follows: During Riks analysis, the tensile strains of the most stressed parts are monitored at every increment. When the tensile strain at the most stressed part reaches the maximum allowable strain value, then the analysis is terminated. If at that increment the load-displacement curve is on the descending branch, then the maximum load that was attained at smaller strains is defined as the failure load and the associated failure mode is plastic hinge formation. If the increment at which the maximum allowable strain is reached corresponds to the ascending branch of the load-deflection curve, hence the formation of plastic hinges has not been completed and the structure can hence support additional load, then the load at the analysis termination is considered as the failure load and the associated failure mode is tensile fracture. This is due to the fact that the main assumption behind plastic analysis is that the plastic hinges possess sufficient ductility/rotation capacity for moment redistribution to occur whilst maintaining their plastic moment resistance, which is clearly not the

case when tensile fracture occurs prior to the required rotation capacity for a collapse mechanism to occur is reached.

The numerically obtained failure loads (F_u) along with the corresponding tensile strains (ε_u) at the most stressed part of the structure and the type of failure are presented in Table 4. To allow comparison among the results, the ratios F_u/F_{el} where F_{el} is the load that causes the bending moment of the most stressed cross-section, as determined by elastic analysis, to reach its respective moment resistance (i.e. plastic moment resistance M_{pl} for Class 1 and 2 sections, elastic moment resistance M_{el} for Class 3 sections) are also included in Table 4. For example, for the specimen S460 100×50×3-LC2, the maximum load P achieved numerically was due to plastic hinge formation and was equal to 74.6 kN ($=F_u$) and the corresponding tensile strain at the top of the cross-section at the central support was equal to 5.8% ($=\varepsilon_u$). For the same specimen, F_{el} is the load for which the S460 100×50×3 cross-section, which is classified as Class 1, achieves its plastic moment resistance (M_{pl}=12.75 kNm), according to the bending moment diagram of Figure 5(b), and is equal to 56.7 kN.

Typical load-displacement curves are shown in Figure 6, where the horizontal axis corresponds to the vertical displacement of the most loaded span in LC1 and the average mid-span vertical displacement in LC2. Note that for the cases that failure was associated with tensile fracture (e.g. 122×50×5 for Figure 6a, 50×50×3, 50×50×4 and 50×50×5 for Figure 6b, 100×50×4 and 100×50×5 for Figure 6c and Figure 6d), the analysis has been terminated at failure. Typical failure modes for both load cases along with the location of the first plastic hinge are depicted in Figure 7.

Table 4. Results of FE parametric study.

	Steel grade	Specimen	F_u (kN)	F_u/F_{el}	ε_u	Failure mode
LC1	S460	50 × 50 × 2	11.8	1.06	4.4%	Plastic hinges
		50 × 50 × 3	20.2	1.30	14.8%	Tensile fracture
		50 × 50 × 4	27.4	1.41	14.8%	Tensile fracture
		50 × 50 × 5	33.8	1.49	14.8%	Tensile fracture
	S690	50 × 50 × 2	17.7	1.19	2.5%	Plastic hinges
		50 × 50 × 3	27.1	1.10	7.5%	Tensile fracture
		50 × 50 × 4	35.5	1.15	7.5%	Tensile fracture
		50 × 50 × 5	42.7	1.19	7.5%	Tensile fracture
	S460	100 × 50 × 2	32.7	1.06	2.4%	Plastic hinges
		100 × 50 × 3	54.3	1.22	4.7%	Plastic hinges
		100 × 50 × 4	79.2	1.39	11.4%	Plastic hinges
		100 × 50 × 5	96.5	1.43	14.8%	Tensile fracture
	S690	100 × 50 × 2	48.8	1.23	2.0%	Plastic hinges
		100 × 50 × 3	77.0	1.10	4.2%	Plastic hinges
		100 × 50 × 4	105.0	1.18	6.8%	Plastic hinges
		100 × 50 × 5	125.6	1.18	7.5%	Tensile fracture
	S460	122 × 50 × 2	42.9	1.02	1.9%	Plastic hinges
		122 × 50 × 3	67.8	1.11	3.3%	Plastic hinges
		122 × 50 × 4	103.8	1.32	8.9%	Plastic hinges
		122 × 50 × 5	135.6	1.43	14.8%	Tensile fracture
	S690	122 × 50 × 2	63.5	1.20	1.8%	Plastic hinges
		122 × 50 × 3	96.1	1.00	2.5%	Plastic hinges
		122 × 50 × 4	140.3	1.14	4.7%	Plastic hinges
		122 × 50 × 5	172.7	1.16	7.5%	Tensile fracture
LC2	S460	50 × 50 × 2	16.3	1.15	3.7%	Plastic hinges
		50 × 50 × 3	27.7	1.39	14.8%	Tensile fracture
		50 × 50 × 4	37.6	1.52	14.8%	Tensile fracture
		50 × 50 × 5	47.6	1.64	14.8%	Tensile fracture
	S690	50 × 50 × 2	24.8	1.30	2.9%	Plastic hinges
		50 × 50 × 3	36.9	1.18	7.5%	Tensile fracture
		50 × 50 × 4	47.5	1.20	7.5%	Tensile fracture
		50 × 50 × 5	55.6	1.20	7.5%	Tensile fracture
	S460	100 × 50 × 2	45.1	1.15	3.8%	Plastic hinges
		100 × 50 × 3	74.6	1.32	5.8%	Plastic hinges
		100 × 50 × 4	101.8	1.41	14.8%	Tensile fracture
		100 × 50 × 5	126.0	1.45	14.8%	Tensile fracture
	S690	100 × 50 × 2	68.0	1.35	2.8%	Plastic hinges
		100 × 50 × 3	105.5	1.18	4.1%	Plastic hinges
		100 × 50 × 4	138.0	1.20	7.5%	Tensile fracture
		100 × 50 × 5	166.0	1.20	7.5%	Tensile fracture
	S460	122 × 50 × 2	59.7	1.11	3.4%	Plastic hinges
		122 × 50 × 3	96.5	1.23	5.7%	Plastic hinges
		122 × 50 × 4	143.5	1.43	9.9%	Plastic hinges
		122 × 50 × 5	178.5	1.47	14.8%	Tensile fracture
	S690	122 × 50 × 2	87.4	1.28	1.6%	Plastic hinges
		122 × 50 × 3	141.6	1.15	5.2%	Plastic hinges
		122 × 50 × 4	190.8	1.20	7.4%	Plastic hinges
		122 × 50 × 5	235.6	1.23	7.5%	Tensile fracture

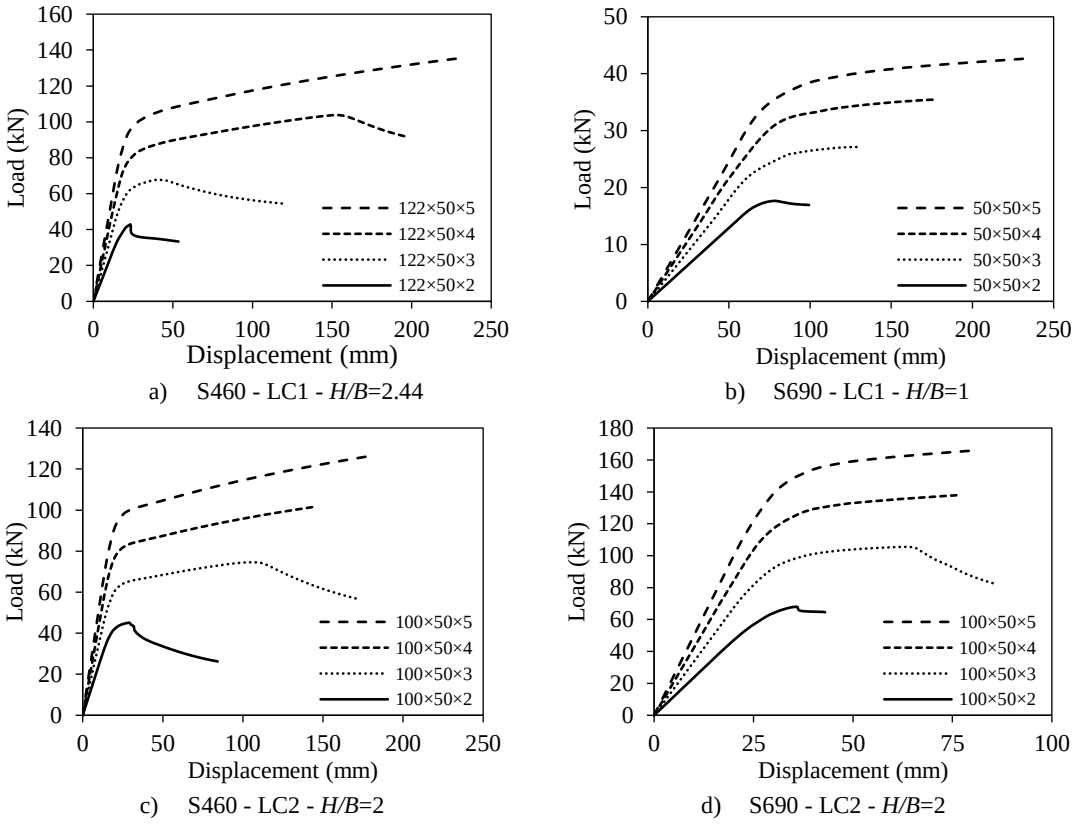

a) S460 - LC1 - *H/B*=2.44

b) S690 - LC1 - *H/B*=1

c) S460 - LC2 - *H/B*=2

d) S690 - LC2 - *H/B*=2

Figure 6. Typical load-displacement curves.

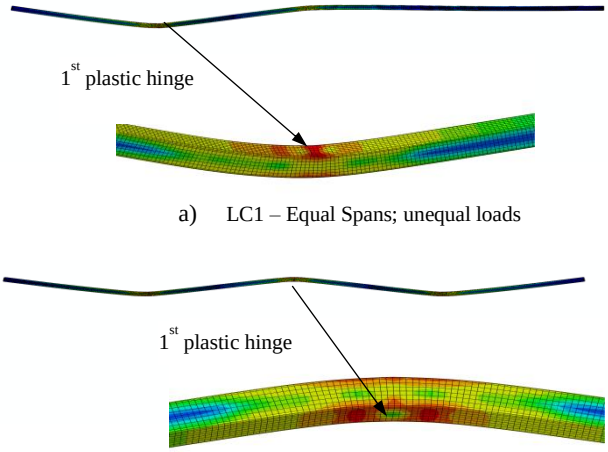

a) LC1 – Equal Spans; unequal loads

b) LC2 – Equal spans; equal loads

Figure 7. Numerically generated failure modes.

In order to evaluate the effect of key parameters on the ultimate response, the average values of the attained normalised load ratios and the ultimate strains at failure are summarised in Table 5. As anticipated, owing to their more favourable strain-hardening and ductility, S460 continuous beams have higher normalised loads and larger ultimate strains than their S690 counterparts. Moreover, as expected, the increase in the cross-sectional thickness leads gradually to larger normalised loads and ultimate strains. This is in line with the general trend demonstrated in Table 4, with plastic hinge formation being the cause of failure for more slender sections and tensile fracture for more stocky sections. Finally, the achieved normalised load ratios and the corresponding strains improve for decreasing aspect ratios. This can be related with the beneficial effects of plate element interaction on the local buckling performance of the compression flange at the plastic hinge formation. This conclusion is again in line with the last column of Table 4, where it can be observed that for example the SHS with thickness of 3 mm (for both steel grades and for both load cases) failed due to tensile fracture, while their RHS counterparts failed due to plastic hinge formation.

Table 5. Effect of key factors on ultimate response of continuous beams.

Key factors		average F_u/F_{el}	average ε_u
Steel grade	S460	1.29	9.69%
	S690	1.18	5.45%
Thickness	t=2	1.17	2.77%
	t=3	1.18	6.67%
	t=4	1.28	9.68%
	t=5	1.32	11.16%
Aspect Ratio	H/B=1.0	1.26	9.22%
	H/B=2.0	1.24	7.19%
	H/B=2.44	1.20	6.30%

4.2 Design recommendations

4.2.1 Eurocode - *Clause 5.4.3(1) of [1]*

As previously mentioned, EN 1993-1-12 [1] does not allow plastic design for HSS indeterminate structures. Hence, according to EN 1993-1-1 [2] the ultimate load that a continuous beam can carry is the one that causes the bending moment of the most stressed cross-section, as determined by elastic analysis, to reach its respective moment resistance not allowing for moment redistribution.

4.2.2 Proposed plastic design method

In order to assess the applicability of the traditional plastic design for Class 1 high strength steel sections, a variation of the current Eurocode method for carbon steel structures, which allows Class 1 sections to be plastically designed (F_{pl}), assuming rigid-plastic material response, is evaluated. This method is expected to lead to improved predictions for Class 1 sections. For the evaluation of F_{pl}, all possible collapse mechanisms of the continuous beams are considered and the respective collapse loads are evaluated by equating the internal work, i.e. work done by the moments at the plastic hinges and determined as the product of the plastic moment M_{pl} and the corresponding rotation θ at the plastic hinges, with the external work determined as the product of the external load P and the corresponding vertical displacement δ. The smallest load resulting from all possible collapse mechanisms is the collapse load F_{pl}. For the present study, the ratio F_{pl}/F_{el} is equal to 1.08 and 1.13 for LC1 and LC2 respectively.

4.2.3 Assessment of Eurocode elastic design method and the proposed plastic design method

The ultimate capacity predictions (F_{pred}) determined according to the two design methods outlined above (i.e. elastic design, plastic design) are normalised by the failure loads (F_u) and the obtained ratios together with the cross-section classes are shown in Table 6. It can be seen that the elastic design method suggested by Eurocode yields more conservative design predictions (mean F_{pred}/F_u equal to 0.81), while more accurate design predictions with a mean normalised ratio closer to unity (mean F_{pred}/F_u equal to 0.88) are obtained if moment redistribution is allowed in the proposed plastic design method. Similar conclusions can be drawn from Figure 8, where the normalised loads are plotted against the $c/t\varepsilon$. The current Eurocode classification limits [2] are also included in the same figure. The design estimations based on the proposed plastic method, are closer to the F_{pred}/F_u unity line, thus implying its accuracy compared to the elastic method suggested by Eurocode. As anticipated, the results appear largely scattered, owing to the fact that the material strain-hardening evident in stocky sections is not taken into account in Eurocode. The same effect has been extensively shown for stainless steel beams [28, 29] where the strain-hardening properties

are pronounced. For the cross-sections that fall within Class 3 (i.e. $38 \leq c/t\varepsilon < 42$), the elastic method only applies, thereby leading to more conservative design estimations (i.e. lower F_{pred}/F_u ratios). With only few results providing marginally unsafe predictions for the plastic design method, the present study encourages further investigation into the possibility of applying plastic design to high strength steels.

Table 6. Eurocode assessment for the design of HSS continuous beams.

	Steel grade	Specimen	Class	F_{pred}/F_u	
				Elastic design	Plastic design
LC1	S460	50 × 50 × 2	1	0.94	1.02
		50 × 50 × 3	1	0.77	0.83
		50 × 50 × 4	1	0.71	0.77
		50 × 50 × 5	1	0.67	0.73
	S690	50 × 50 × 2	3	0.84	0.84
		50 × 50 × 3	1	0.91	0.98
		50 × 50 × 4	1	0.87	0.94
		50 × 50 × 5	1	0.84	0.91
	S460	100 × 50 × 2	1	0.94	1.02
		100 × 50 × 3	1	0.82	0.88
		100 × 50 × 4	1	0.72	0.77
		100 × 50 × 5	1	0.70	0.76
	S690	100 × 50 × 2	3	0.81	0.81
		100 × 50 × 3	1	0.91	0.98
		100 × 50 × 4	1	0.85	0.92
		100 × 50 × 5	1	0.85	0.92
	S460	122 × 50 × 2	2	0.98	0.98
		122 × 50 × 3	1	0.90	0.97
		122 × 50 × 4	1	0.76	0.81
		122 × 50 × 5	1	0.70	0.75
	S690	122 × 50 × 2	3	0.83	0.83
		122 × 50 × 3	1	1.00	1.08
		122 × 50 × 4	1	0.88	0.95
		122 × 50 × 5	1	0.86	0.93
LC2	S460	50 × 50 × 2	1	0.87	0.98
		50 × 50 × 3	1	0.72	0.81
		50 × 50 × 4	1	0.66	0.75
		50 × 50 × 5	1	0.61	0.69
	S690	50 × 50 × 2	3	0.77	0.77
		50 × 50 × 3	1	0.85	0.96
		50 × 50 × 4	1	0.83	0.93
		50 × 50 × 5	1	0.83	0.93
	S460	100 × 50 × 2	1	0.87	0.98
		100 × 50 × 3	1	0.76	0.86
		100 × 50 × 4	1	0.71	0.80
		100 × 50 × 5	1	0.69	0.78
	S690	100 × 50 × 2	3	0.74	0.74
		100 × 50 × 3	1	0.85	0.95
		100 × 50 × 4	1	0.83	0.93
		100 × 50 × 5	1	0.83	0.93
	S460	122 × 50 × 2	2	0.90	0.90
		122 × 50 × 3	1	0.81	0.91
		122 × 50 × 4	1	0.70	0.79
		122 × 50 × 5	1	0.68	0.76
	S690	122 × 50 × 2	3	0.78	0.78
		122 × 50 × 3	1	0.87	0.98
		122 × 50 × 4	1	0.83	0.93
		122 × 50 × 5	1	0.81	0.91
		Mean		0.81	0.88
		COV		0.11	0.11

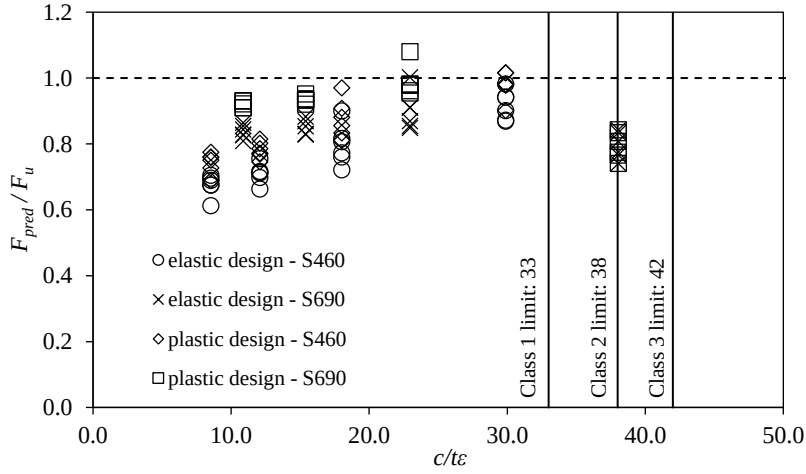

Figure 8. Normalised load vs cross-section slenderness.

4.3 Reliability analysis

A statistical analysis in accordance with the provisions of Annex D of EN 1990 [38] has been conducted in order to assess the reliability of the elastic and plastic design methods for HSS indeterminate structures. In this analysis, Class 1 sections, which are those that may be plastically designed, have been considered. For the execution of a first-order reliability method in accordance with the Eurocode target reliability requirements, the following steps were applied:

- Development of a model for the predicted values (r_t)
- Comparison between numerical (r_e) to predicted (r_t) values
- Estimation of the average ratio $\bar{b}$ of the numerical (r_e) to predicted (r_t) resistance based on a least-squares fit to the data
- Estimation of the coefficient of variation (V_δ) through the determination of the error term (δ_i)
- Definition of the combined CoV incorporating both model and basic variable uncertainties (V_r). In line with the considerations in [13], the CoV of geometric properties was taken equal to 0.02, whereas the material over-strength of HSS equal to 1.135 with a CoV of 0.055. Based on the validation of the numerical models presented in [21], the variation between the experimental and the numerical results was considered equal to 0.05.
- Definition of the characteristic C_k and the design value C_d as a function of the design (ultimate limit state) fractile factor ($k_{d,n}$)
- Evaluation of the partial safety factor γ_{M0}

The numerical values plotted against the predicted ones are shown in Figure 9, where n the number of FE simulations used in the reliability analysis. Table 7 summarises the key statistical parameters. As can be seen, even though the Eurocode elastic design method is more conservative ($\bar{b}$=1.405) compared to the proposed plastic design method ($\bar{b}$=1.118), it is associated with a larger required partial safety factor γ_{M0}.

This is because the elastic design method leads to largely scattered predictions, particularly conservative for sections with decreasing slenderness, whereas the proposed plastic design method provides more accurate and more consistent capacity predictions, as it allows for moment redistribution. Although the required γ_{M0} factor for plastic design is slightly higher than unity (1.06), thus indicating that the required reliability is not achieved, due to the fact that the relevant partial safety factor for elastic design is significantly higher (1.21), plastic design is deemed safe. The improved consistency of the predictions according to the plastic design method encourages further the prospect of adopting plastic design rules for HSS indeterminate structures.

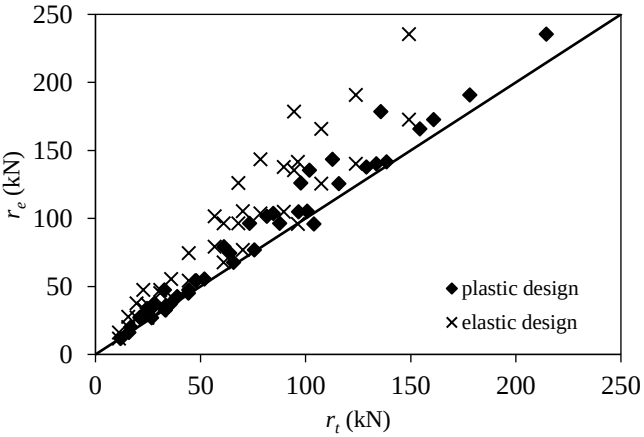

Figure 9. Comparison of numerical loads r_e and predicted resistances r_t.

Table 7. Reliability analysis for elastic and plastic design.

	n	$k_{d,n}$	$\bar{b}$	V_δ	V_r	γ_{M0}
elastic design	40	3.354	1.405	0.193	0.210	1.21
plastic design	40	3.354	1.118	0.112	0.139	1.06

5 CONCLUSIONS

A comprehensive study on the numerical response of two-span continuous beams employing hot-finished square and rectangular hollow sections in S460 and S690 steel grades has been carried out. The obtained results were analysed and relevant design specifications were evaluated, extending the pool of available structural performance HSS data. The possibility of applying plastic design to HSS indeterminate structures, currently not allowed by EN 1993-1-12 [1], has been studied, showing that plastic design could be applied for the presently studied cross-sections and thus this possibility should be considered and further explored. The present paper aims to contribute to the development of more advanced design specifications for HSS, in line with their observed structural response, and potentially lead to an increased usage of HSS in the construction sector.

ACKNOWLEDGMENTS

The research leading to these results has received funding from the Research Fund for Coal and Steel (RFCS) under grant agreement No. RFSR CT 2012-00028.

REFERENCES

[1] EN 1993-1-12 (2007) Eurocode 3: Design of steel structures, Part 1-12: Additional rules for the extension of EN 1993 up to steel grades S 700. Brussels: European Committee for Standardization (CEN).

[2] EN 1993-1-1 (2014) BS EN 1993-1-1: 2005+A1:2014, Eurocode 3 : design of steel structures, Part 1-1: general rules and rules for buildings. London: BSI.

[3] Zhou, F., Tong, L. and Chen, Y. (2013) Experimental and numerical investigations of high strength steel welded H-section columns. International Journal of Steel Structures, 13(2): 209-218.

[4] Ban, H., Shi, G., Shi, Y. and Bradford, M.A. (2013) Experimental investigation of the overall buckling behaviour of 960MPa high strength steel columns. Journal of Constructional Steel Research, 88: 256-266.

[5] Somodi, B. and Kövesdi, B. (2017) Flexural buckling resistance of cold-formed HSS hollow section members. Journal of Constructional Steel Research, 128: 179-192.

[6] Somodi, B. and Kövesdi, B. (2017) Flexural buckling resistance of welded HSS box section members. Thin-Walled Structures, 119: 266-281.

[7] Wang, Y. B., Li, G. Q., Chen, S. W. and Sun, F. F. (2014) Experimental and numerical study on the behavior of axially compressed high strength steel box-columns. Engineering Structures, 58: 79-91.

[8] Kim, D.K., Lee, C.H., Han, K.H., Kim, J.H., Lee, S.E. and Sim, H.B. (2014) Strength and residual stress evaluation of stub columns fabricated from 800MPa high-strength steel. Journal of Constructional Steel Research, 102: 111-120.

[9] Lee, C. H., Han, K. H., Uang, C. M., Kim, D. K., Park, C. H. and Kim, J. H. (2012) Flexural strength and rotation capacity of I-shaped beams fabricated from 800-MPa steel. Journal of Structural Engineering, 139(6): 1043-1058.

[10] Schillo, N. and Feldmann, M. (2016) The rotational capacity of beams made of high-strength steel. Proceedings of the Institution of Civil Engineers-Structures and Buildings, 170(9): 641-652.

[11] Pavlovic, M. and Veljkovic, M. (2017) Compact cross-sections of mild and high-strength steel hollow section beams. Proceedings of the Institution of Civil Engineers-Structures and Buildings, 170(11): 825-840.

[12] Zhao, X. L. (2000) Section capacity of very high strength (VHS) circular tubes under compression. Thin-Walled Structures, 37(3): 223-240.

[13] Ma, J. L., Chan, T. M. and Young, B. (2018) Design of Cold-Formed High-Strength Steel Tubular Stub Columns. Journal of Structural Engineering, 144(6): 04018063.

[14] Rasmussen, K.J.R. and Hancock, G.J. (1995) Tests of high strength steel columns. Journal of Constructional Steel Research, 34: 27-52.

[15] Wang, Y.B., Li, G.Q. and Chen, S.W. (2012) Residual stresses in welded flame-cut high strength steel H-sections. Journal of Constructional Steel Research, 79: 159-165.

[16] Wang, Y.B., Li, G.Q. and Chen, S.W. (2012) The assessment of residual stresses in welded high strength steel box sections. Journal of Constructional Steel Research, 76: 93-99.

[17] Wang, J., Afshan, S., Schillo, N., Theofanous, M., Feldmann, M. and Gardner, L. (2017) Material properties and compressive local buckling response of high strength steel square and rectangular hollow sections. Engineering Structures, 130: 297-315.

[18] Gkantou, M., Theofanous, M., Antoniou, N. and Baniotopoulos, C. (2017) Compressive behaviour of high strength steel cross-sections. Proceedings of the Institution of Civil Engineers–Structures and Buildings. http://dx.doi.org/10.1680/jstbu.16.00101.

[19] Wang, J., Afshan, S., Gkantou, M., Theofanous, M., Baniotopoulos, C. and Gardner, L. (2016) Flexural behaviour of hot-finished high strength steel square and rectangular hollow sections. Journal of Constructional Steel Research, 121: 97-109.

[20] Gkantou, M., Theofanous, M., Wang, J., Baniotopoulos, C. and Gardner, L. (2017) Behaviour and design of high strength steel cross-sections under combined loading. Proceedings of the Institution of Civil Engineers–Structures and Buildings. http://dx.doi.org/10.1680/jstbu.16.00114.

[21] Gkantou, M., Theofanous, M. and Baniotopoulos, C. (2017) Structural response of square and rectangular high strength steel hollow sections under combined biaxial bending and compression. In the Proceedings of the 8th European Conference on Steel and Composite Structures. Copenhagen (Denmark), September 13-15.

[22] Wang, J. and Gardner, L. (2017). Flexural buckling of hot-finished high-strength steel SHS and RHS columns. Journal of Structural Engineering, 143(6): 04017028.

[23] Yang, C.H., Beedle, L.S. and Johnston, B.G. (1952) Residual stress and the yield strength of steel beams. Weld. J., 31(4): 205-229.

[24] Popov, E.P and Willis, J.A (1957) Plastic design of cover plated continuous beams. Journal of the Engineering Mechanics Division, 84(1): 1495-1515.

[25] De Luca, A. (1982) Inelastic Behavior of Aluminum Alloy Continuous Beams. Rep. No. 506, Institute of Technology and Constructions, Naples, Italy.

[26] Su, M. N., Young, B. and Gardner, L. (2014) Continuous beams of aluminum alloy tubular cross sections. I: tests and FE model validation. Journal of Structural Engineering, 141(9): 04014232.

[27] Su, M. N., Young, B., and Gardner, L. (2014) Continuous beams of aluminum alloy tubular cross sections. II: parametric study and design. Journal of Structural Engineering, 141(9): 04014233.

[28] Theofanous, M., Saliba, N., Zhao, O., and Gardner, L. (2014) Ultimate response of stainless steel continuous beams. Thin-Walled Structures, 83: 115-127.

[29] Arrayago, I., Real, E., and Mirambell, E. (2017) Design of stainless steel continuous beams with tubular cross-sections. Engineering Structures, 151: 422-431.

[30] Gkantou, M., Kokosis, G., Theofanous, M. and Dirar, S. (2018) Plastic design of stainless steel continuous beams. Journal of Constructional Steel Research. https://doi.org/10.1016/j.jcsr.2018.03.025.

[31] EN 1993-1-5 (2006) Eurocode 3: Design of steel structures – Part 1-5: Plated structural elements. Brussels: European Committee for Standardization (CEN).

[32] Sedlacek, G. and Feldmann, M. (1995) Background document 5.09 for chapter 5 of Eurocode 3 Part 1.1: the b/t ratios controlling the applicability of analysis models in Eurocode 3 Part 1.1. Technical report. Aachen.

[33] Hibbitt, Karlsson & Sorensen and Inc (2012) ABAQUS. ABAQUS/Standard User's Manual Volumes I–III and ABAQUS CAE Manual. Pawtucket, USA: Dassault Systèmes.

[34] Tran, A.T., Veljkovic, M., Rebelo, C. and da Silva, L.S. (2016) Resistance of cold-formed high strength steel circular and polygonal sections - Part 2: Numerical investigations. Journal of Constructional Steel Research, 125: 227-238.

[35] Zhou, F., Tong, L. and Chen, Y. (2013) Experimental and numerical investigations of high strength steel welded H-section columns. International Journal of Steel Structures, 13: 209-218.

[36] Ellobody, E., Ran Feng, A. and Young, B. (2013) Finite element analysis and design of metal structures. Elsevier.

[37] Kokosis, G., Gkantou, M. and Theofanous, M. (2017) Ultimate response and design of stainless steel continuous beams. In the Proceedings of the 8th European Conference on Steel and Composite Structures. Copenhagen (Denmark), September 13–15.

[38] EN 1990 (2002) Eurocode–basis of structural design. Brussels: European Committee for Standardization (CEN).